

# Time Series Imaging for Link Layer Anomaly Classification in Wireless Networks

Blaž Bertalaníč, *Graduate Student Member, IEEE*, Marko Meža, *Senior member, IEEE*, and Carolina Fortuna

**Abstract**—The number of end devices that use the last mile wireless connectivity is dramatically increasing with the rise of smart infrastructures and require reliable functioning to support smooth and efficient business processes. To efficiently manage such massive wireless networks, more advanced and accurate network monitoring and malfunction detection solutions are required. In this paper, we perform a first time analysis of image-based representation techniques for wireless anomaly detection using recurrence plots and Gramian angular fields and propose a new deep learning architecture enabling accurate anomaly detection. We examine the relative performance of the proposed model and show that the image transformation of time series improves performance of anomaly detection by up to 29% for binary classification and by up to 27% for multiclass classification. At the same time, the best performing model based on recurrence plot transformation leads to up to 55% increase compared to the state of the art where classical machine learning techniques are used. We also provide insights for the decisions of the classifier using an instance based approach enabled by insights into guided back-propagation. Our results demonstrate the potential of transformation of time series signals to images to improve classification performance compared to classification on raw time series data.

**Index Terms**—anomaly detection, wireless networks, link layer, imaging, time-series, classification, Gramian angular field, recurrence plot, machine vision, deep learning.

## I. INTRODUCTION

WIRELESS networks represent the most convenient last mile connectivity solution and are used daily by billions of devices such as phones, tablets, laptops, desktops and increasingly smart devices forming the so-called Internet of Things [1]. Traditionally, last mile connectivity issues were resolved by the owner of the access point be it an individual person, a cable or other operator in case of non-cellular operators, base station in the case of cellular only operators in a *reactive* and *mostly manual* manner. The reactivity is due to the fact that the entire model assumed that the customers would notice problems and take action by notifying the operators or resetting and reconfiguring equipment when possible. The manual mitigation is mostly due to the fact that the entire network, including the wired-to-wireless converter used static, *pre-configured specialized* hardware equipment.

With the increased digitization of society, including cities and infrastructures such as transportation and energy, the number of end devices that use the last mile wireless connectivity is dramatically increasing and often require reliable functioning to support smooth and efficient business processes. Furthermore, the wired-to-wireless converters as well as the core transport networks are migrating to *software controlled virtual functions residing on top of more general purpose hardware* leading to increasingly complex and expensive network

operation. For instance, as shown in Figure 1 and specified in the technical annex of the 3GPP 5G standard<sup>1</sup>, an end-to-end network slice (i.e. virtual network service) can be created in a matter of minutes. The operational slices need to be continuously monitored throughout their lifetime and reconfigured as needed, possibly in a fully automatic manner, by the slice orchestrator in the OSS/BSS (operations/business support systems, respectively) of the network operators. The software and virtualization driven agility and complexity of the emerging networks requires faster configuration and reaction times. For instance, the automatic selection of a frequency band to be used at a given time and place should be suitably informed by events in the radio spectrum, automatically detected by automatic spectrum sensing, detection and classification systems [2], while the transmission parameters such as transmit power and channel number could be selected according to the perceived link quality [3]. Finally, when a link outage or an abnormal network behaviour occurs, it should be proactively detected and fixed before it causes significant user dissatisfaction [4] using network monitoring [5] and malfunction detection [6] solutions that automatically report relevant issues that can be mitigated without disrupting the business process.

An anomaly in general can be defined from a mathematical perspective as a rare event or an outlier of a distribution. Several machine learning techniques have been developed to detect such outliers and they typically use an unsupervised machine learning approach. For instance a typical example of such rare, unknown events that cannot be easily characterized a-priori is intrusion detection. Most such recent anomaly detections are performed on multivariate time series data [7], [8], [9], [10] using unsupervised deep learning algorithms in the form of autoencoder networks.

An anomaly can also be defined from an application perspective as being an event that causes inconvenience to the respective application. The respective event does not necessarily need to be rare from a mathematical point of view, and its characterization is often known. For instance, Sheth *et al.* [6] define and identify anomalies from the IEEE 802.11 physical layer perspective, namely, hidden terminal, capture effect, noise and signal strength variation anomalies, whereas Gupta *et al.* [11] define anomalies from multihop networking perspective with the aspects, such as black hole, sink hole, selective forwarding and flooding. More recently, starting from observable symptoms of link measurements, namely the changes in the expected received signal, [4] proposed four types of link layer anomalies, namely sudden degradation (SuddenD), sudden

<sup>1</sup>3rd Generation Partnership Project, <https://www.3gpp.org/>

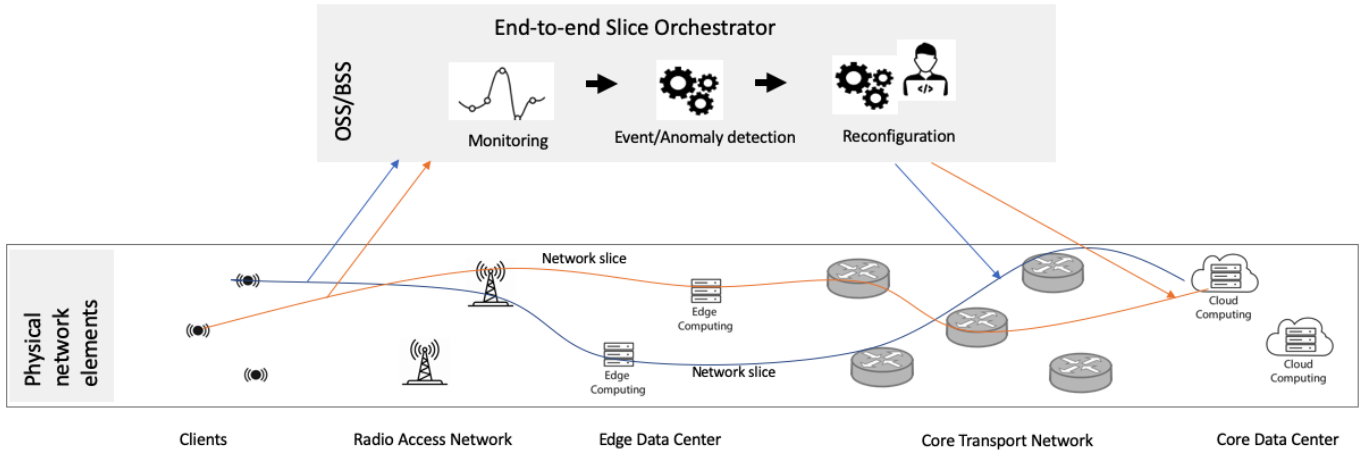


Fig. 1. Example emerging wireless end-to-end slices and the role of automatic anomaly detection for the slice orchestrator.

degradation with recovery (SuddenR), instantaneous degradation (InstaD) and slow degradation (SlowD). They were the first to evaluate different time series representations such as Fast Fourier Transform (FFT), histogram, aggregates and compressed autoencoded in an attempt to develop a classifier for the defined anomalies. However, their approach only used classical, non deep learning methods and in developing them they made assumptions that are not entirely aligned with a realistic environment where various anomalies can appear simultaneously on links rather than isolated.

Inspired by the breakthroughs in image recognition [12] and object recognition [13] that have been going on over the last decade, and attempts from various fields of science in formulating domain specific problems as image problems to benefit from these achievements [14], [15], we also endeavour in the first attempt to investigate image base transformations for supervised anomaly detection for wireless links as defined in [4]. In this paper, we propose a new system for anomaly classification in wireless networks based on a time-series to image transformation and deep learning model. The contributions of this paper are:

- We perform a first-time analysis of image based representation for wireless link layer anomaly detection. For this, we consider the four anomaly shapes defined in [4], the recently introduced Gramian angular fields [16] (GAF) and recurrence plots [17].
- We propose deep neural network models for classification of the four types of anomalies and show that it outperforms the state of the art.
- Provide insights for the decisions of the classifier using an instance based approach enabled by insights into guided back-propagation.

This paper is organized as follows. We discuss related work in Section II. Section III provides the formal problem statement, while Section IV elaborates on various time series transformations that can be used to generate image representations. Section V introduces the proposed deep learning models, Section VI describes the relevant methodological and experimental details, while Section VII provides thorough analyses of the results. Finally, Section VIII concludes the paper.

## II. RELATED WORK

To support our contributions and put our work in perspective, we first analyse related work with respect to time series classification and then narrow down to works on image transformation for anomaly detection.

### A. Time series classification in general

Unlike other type of data, time series contain ordered values and classification algorithms need to take this into account [18]. Begnall *et al.* [19] collected and investigated ways in which time series can be compared or classified into the correct class. Time series traces can be compared as a whole or by intervals, short patterns with shapelets can be detected, or a dictionary approach can be employed where the frequency of repetition of subseries is modelled and classifiers are built based on the resulting histograms. A combination of all the previous methods can also be used as well as a customized model for each series and then measure similarities. With this in mind, Xing *et al.* [20] divided time series classification (TCS) methods into three main categories: model-based, feature-based as used in this work, and distance-based methods.

Laengkvist *et al.* [20] divided existing deep learning based models for TSC into two main categories: discriminative models and generative models. The two categories were further subdivided by Fawaz *et al.* [21] into additional subgroups, namely models that use hand-engineering features and direct end-to-end models. End-to-end models are those where the input of a model is raw time series data, while feature engineering models take as input features created by hand through feature extraction, part of which are time series to image transformations. Eckmann *et al.* [17] was probably the pioneer of time series to image transformations by introducing recurrence plots (RP). RPs were used mainly to see the data from a different perspective rather than to solve the classification problem of time series data. However, with DL and convolutional neural networks, RP became interesting for solving time series classification problems as noticed by Wang *et al.* [16]. In the same paper, they also introduced two

other methods of time series to image transformations called Gramian Angular Fields (GAF) and Markov transition field. All three approaches have recently been used as an indirect method for classifying time series data using convolutional neural networks and deep learning networks. There are not many works on using time series to image transform for anomaly detection. All three transformations considered in [16] were also used in solving regression problems [22].

### B. Image transformation for anomaly detection

The most recent usage of images for anomaly detection was presented by Choi *et al.* [23] that used Generative Adversarial Networks to transform multivariate time series into images and to detect and localize anomalies in signals from power-plants. Krummenacher *et al.* [24] did an interesting work on finding anomalies within wheels of train cart wagons by transforming sensor signal into Gramian Angular Field and using convolutional neural networks for detecting defects. One of the first applications of GAF for anomaly detection was attempted by Zhang *et al.* [25] for anomaly detection in EKG signals. Another interesting use of GAF and deep learning (DL) can be found in Xu *et al.* [26] for recognizing human actions with signals received from wearable devices. This kind of classification is gaining momentum in the last few years, but as far as we know, no one used this approach for anomaly detection in wireless signals.

In recent years, some work has also been done on anomaly detection and time series classification using recurrence plots (RP). One of the first works on time series classification was by Silva *et al.* [27], where they showed that transformation to RP improves classification performance on most of the datasets they used for testing. Hu *et al.* [28] proposed a framework for anomaly detection in time series using RP transformation. Another anomaly detection work was done by [29] where they used RP transform and CNN on multisensor signals for real-time anomaly detection in flash butt welding process. In the network domain, an attempt was made by [30] to detect DDoS attacks using RP plots and convolutional neural networks.

## III. PROBLEM FORMULATION

Starting from the example emerging wireless networks and the role of anomaly detection within depicted in Figure 1, we formulate the steps that enable automatic anomaly detection from time series. More specifically, we propose transforming the incoming time series data into images and then training a deep learning model to recognize anomalies in those respective images as depicted in Figure 2 and further explained in this section. The model is then able to automatically classify the images depending on whether they contain anomalies or not.

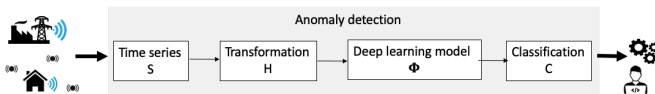


Fig. 2. Wireless link anomaly detection steps.

### A. Classification problem

We formulate the anomaly detection problem as a classification problem in which given an input tensor  $H$ , there is a function  $\Phi$  that maps the input to a set of target classes  $C$  as provided in Equation 1.

$$C = \Phi(H) \quad (1)$$

The cardinality of the set  $C$ , also denoted as  $|C|$ , denotes the number of classes to be recognized. Without loss of generality, in the remainder of the paper we focus on two cases. In the first case, we consider a binary classification problem with  $|C| = 2$  where the set of target classes is  $C = \{anomalous, normal\}$ . In the second case, we start from the four types of anomalies introduced in [4] and consider a five class classification problem with  $|C| = 5$  where the set of target classes is  $C = \{SuddenD, SuddenR, InstaD, SlowD, normal\}$ . The binary classification problem aims to detect whether an incoming portion of a time-series contains or not one the four anomalies. The five class problem aims to detect the specific type of anomaly defined in the literature or a normal link.

For the case of the five class problem, the first anomaly, called Sudden degradation without recovery (SuddenD), is an anomaly where the signal unexpectedly drops to a minimal value and never recovers as depicted in Figure 4a. The second anomaly, called Sudden degradation with recovery (SuddenR), has a certain similarity to SuddenD only that the signal after a certain period of time recovers from minimal back to the normal value as in Figure 5a. The third anomaly that was defined was Instantaneous degradation (InstaD) that shows itself as a spike within a trace. Here the value of a trace drops to a minimal for a very short, instantaneous, amount of time and then recovers back to a normal value as in Figure 6a. The fourth anomaly that was defined is a Slow degradation anomaly (SlowD). This anomaly shows itself in slightly decreasing slope within a trace, where values slowly but gradually decrease like it can be seen in Figure 7a.

### B. Time-series transformation

We define the transformation  $T$  depicted in Figure 2 as a function that transforms the input time series  $S$  to the tensor  $H$  from Eq. 1 as:

$$H = T(S) \quad (2)$$

For multidimensional time series of dimension  $K$ ,  $S$  takes the form of a  $[S]_{K \times N}$  matrix and represents a set of  $K$  time series traces with length  $N$ . In this paper we consider a unidimensional time series where  $K = 1$ , thus  $[S]_{1 \times N}$ . The transformation function  $T$  can be represented by the identity function, in which case the result  $H$  is the same as input time series trace or can represent more complex transformation functions as the ones proposed in this work that transform the time series into images.

## IV. TIME-SERIES TO IMAGE TRANSFORMATION

Section III provided general definition of time series transformation. In the following, we provide two distinct ways to transform time series data representation into images that can be used as features for training deep learning models.

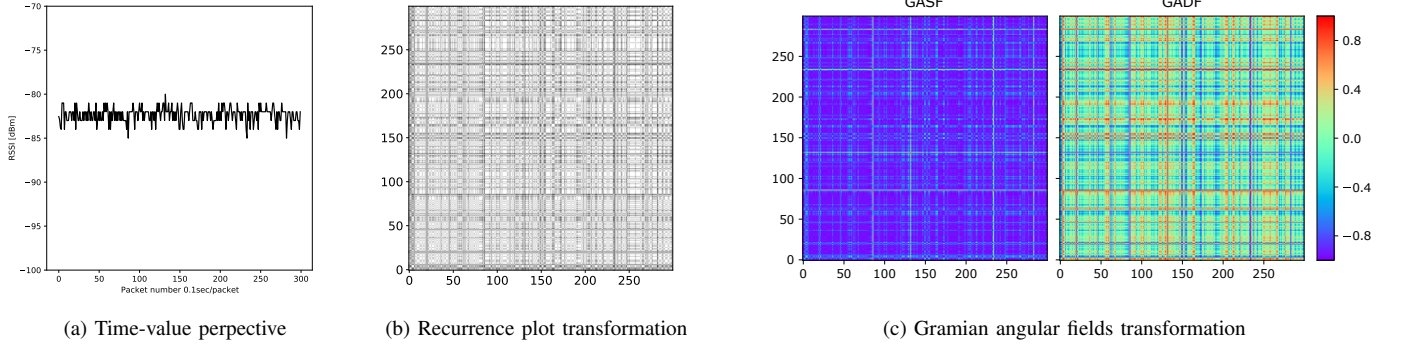


Fig. 3. Distinct representations of the link layer RSSI measurement data without anomaly.

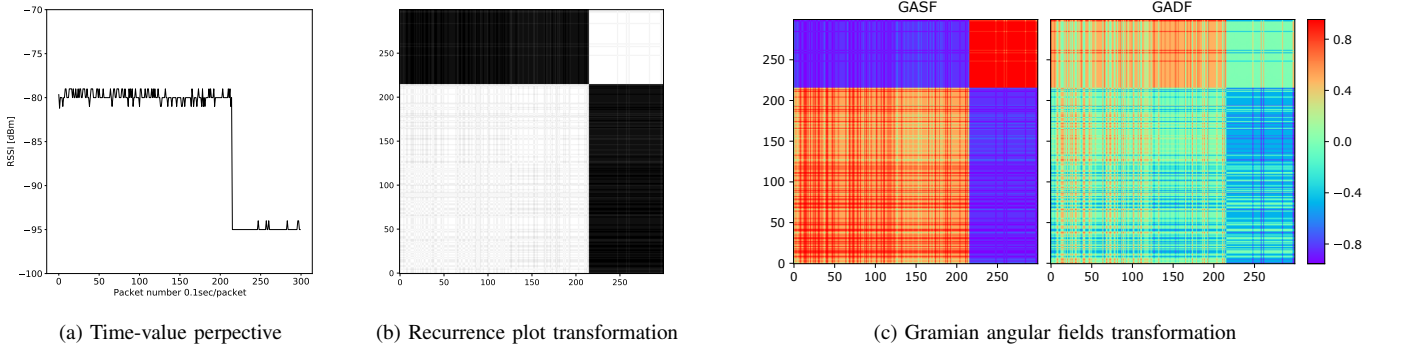


Fig. 4. Distinct representations of the link layer RSSI measurement data for sudden degradation anomaly (SuddenD).

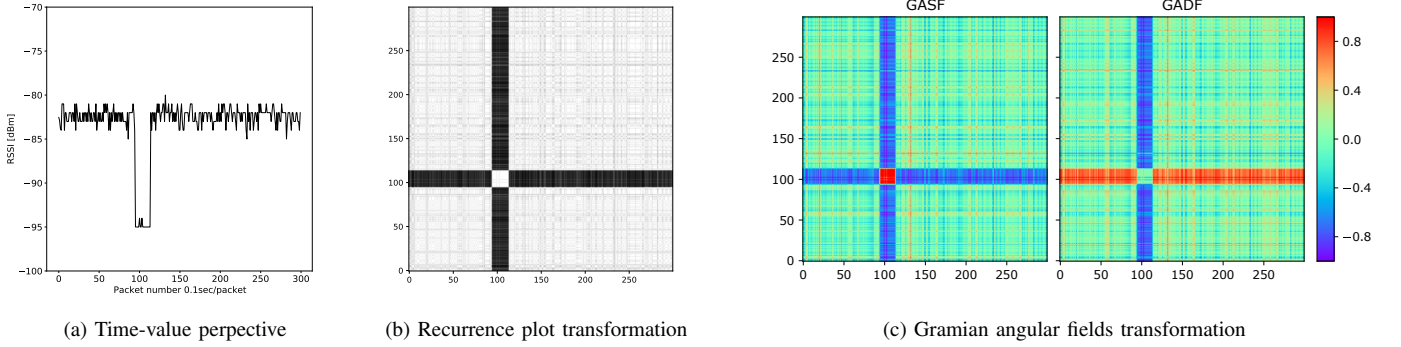


Fig. 5. Distinct representations of the link layer RSSI measurement data for sudden degradation with recovery anomaly (SuddenR).

### A. Recurrence plot transformation

The recurrence plot (RP) is a technique for nonlinear data analysis, that represents a visualisation of a square matrix in which elements correspond to those times steps when parts of a time series are the most similar to each other. The RP transformation takes as its input the matrix representation of unidimensional time series data  $S_{1 \times N}$ , that can be also represented as a vector  $\vec{s}_N$ . This can be seen in the Equation 3, where  $N$  is the length of the time series. According to Equation 4, the absolute value of the difference between two points is computed and represents the distance between the points, which is then subtracted from the predefined threshold

$\epsilon$ . The result  $h$  is then converted to binary values through the use of the Heaviside function  $\Theta$  presented in the Equation 5. The final result is an image  $H$  of size  $N \times N$ . In special cases the threshold and Heaviside function may be omitted resulting in a non binarized matrix of distances between points in the time series.

$$S_{1 \times N} = \vec{s}_N = (s_1, s_2, \dots, s_N) \quad (3)$$

$$h = \epsilon - \begin{pmatrix} \|s_N - s_1\| & \|s_N - s_2\| & \dots & \|s_N - s_N\| \\ \vdots & \vdots & \ddots & \vdots \\ \|s_2 - s_1\| & \|s_2 - s_2\| & \dots & \|s_2 - s_N\| \\ \|s_1 - s_1\| & \|s_1 - s_2\| & \dots & \|s_1 - s_N\| \end{pmatrix} \quad (4)$$



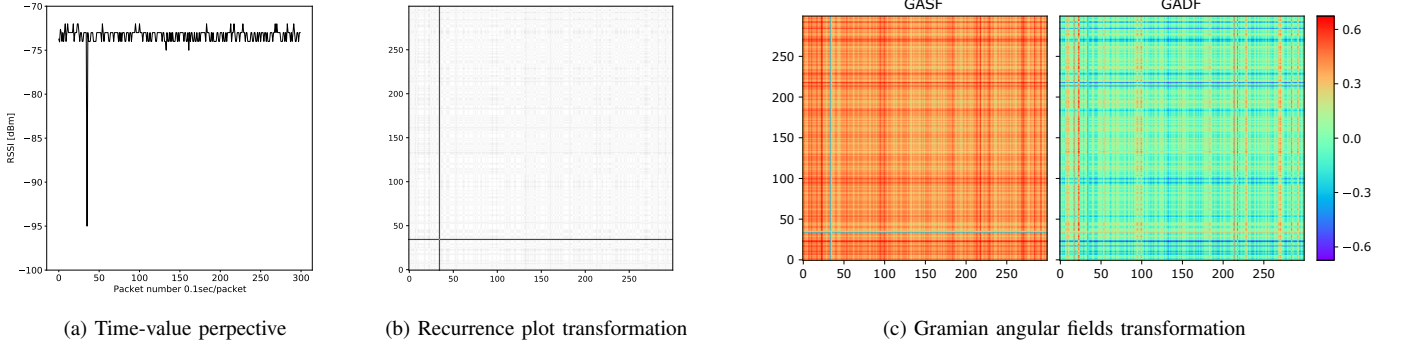


Fig. 6. Distinct representations of the link layer RSSI measurement data for spike-like instantaneous degradation anomaly (InstaD).

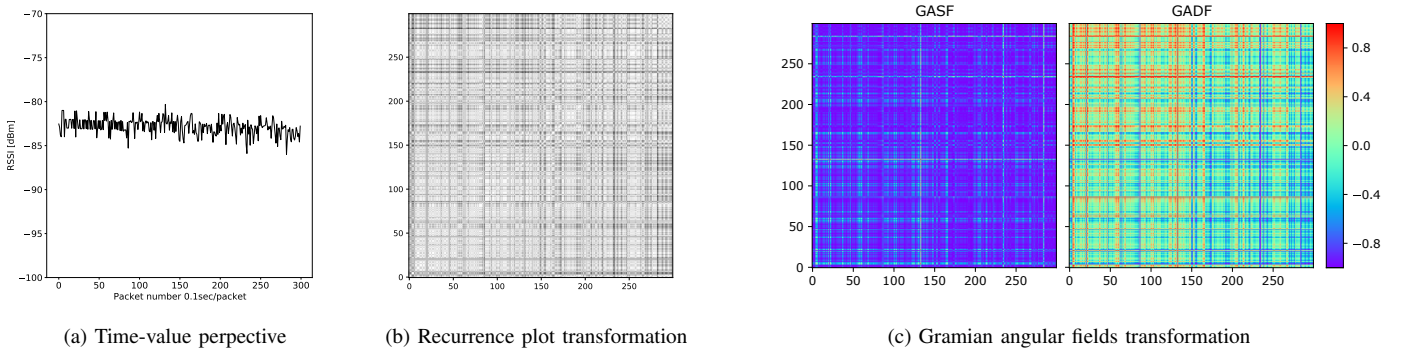


Fig. 7. Distinct representations of the link layer RSSI measurement data for slow degradation anomaly (SlowD).

$$H = \Theta(h) \quad (5)$$

A trace without an anomaly can be seen in Figure 3b. No pattern is apparent, as the arrangement within the image can be labelled as random and correlates with the randomness of the time series representation of the trace. On the other hand, Figure 4b depicts a recurrence plot of the SuddenD anomaly. The typical representation of this anomaly is a white rectangle in the upper right corner. The lower left corner of this rectangle represents the time sample where the anomaly occurred, while the width of the rectangle is the same as the width of the anomaly of the time series anomaly represented in Figure 4a.

Looking at Figure 5b, the SuddenR anomaly appears as a cross that has a small white rectangle in its centre somewhere along the diagonal from the lower left corner to the upper right corner of the image. The lower left corner of the white square represents the beginning of the anomaly, while the upper right corner of the white square shows where the recovery occurred. The size of the rectangle depends on the width of the anomaly.

The third type of anomaly is depicted in Figure 6b. The InstaD anomaly is very similar to the SuddenR anomaly, except that it is much narrower, which is due to its short occurrence within a trace. Just like SuddenR, this anomaly can be observed along the diagonal line from the lower left corner to the upper right corner.

Finally, in Figure 7b, the SlowD anomaly can be observed. This anomaly does not have a typical representation. In some images it is seen as an area of higher point density along

the diagonal from the bottom left to the top right, some have higher density at the top and right edge of the image, while some other images may have a similar distribution as traces without an anomaly. As such, this anomaly with RP transform is harder to detect with the naked eye than others.

### B. Gramian angular field transformation

The Gramian angular field is a transformation of a time series that represents the temporal correlation between points within a time series. The end result is a square image representation of the input time series. This approach consists of two techniques, one is the Gramian angular summation field (GASF) and the other is the Gramian angular difference field (GADF). Both techniques are computed in a similar way. First, the time series needs to be scaled with a min-max normalization and then transformed to a polar coordinate system. The angles  $\phi_N$  from the polar plot are then used to compute GASF and GADF. For the sum field, the angular cosine function of the sum between two points is computed, which is represented in Equation 6, where  $H_S$  represents the GASF transformation. For the GADF representation, the angular sine of the difference between each two points is computed as shown in Equation 7, where  $H_D$  represents the GADF transform. Both GAF representations look similar to those transformed with recurrence plot. The size of the transformed image is  $N \times N$ , where  $N$  represents the length of the time series used in the transformation.

$$H_S = \begin{pmatrix} \cos(\phi_N + \phi_1) & \cos(\phi_N + \phi_2) & \dots & \cos(\phi_N + \phi_N) \\ \vdots & \vdots & \ddots & \vdots \\ \cos(\phi_2 + \phi_1) & \cos(\phi_2 + \phi_2) & \dots & \cos(\phi_2 + \phi_N) \\ \cos(\phi_1 + \phi_1) & \cos(\phi_1 + \phi_2) & \dots & \cos(\phi_1 + \phi_N) \end{pmatrix} \quad (6)$$

$$H_D = \begin{pmatrix} \sin(\phi_N - \phi_1) & \sin(\phi_N - \phi_2) & \dots & \sin(\phi_N - \phi_N) \\ \vdots & \vdots & \ddots & \vdots \\ \sin(\phi_2 - \phi_1) & \sin(\phi_2 - \phi_2) & \dots & \sin(\phi_2 - \phi_N) \\ \sin(\phi_1 - \phi_1) & \sin(\phi_1 - \phi_2) & \dots & \sin(\phi_1 - \phi_N) \end{pmatrix} \quad (7)$$

A trace without an anomaly can be seen in the Figure 3c. Similar to the recurrence plot transformation, there is no obvious pattern in the images and the arrangement also looks random. On the other hand, it can be seen that in Figure 4c that depicts the transformation corresponding to the SuddenD anomaly, a rectangle in the upper right corner of the generated image indicates the anomaly. It can be noticed that the representation is similar to the one generated by the recurrence plot and that it is more visible in the GASF plot rather than the GADF.

Figure 5c depicts the GAF transforms for the SuddenR anomaly. The anomaly appears as a small rectangle somewhere along the diagonal of the image. The width of the rectangle is the same as the width of the anomaly within the time series as can be seen by comparing with the width of the time series anomaly represented in Figure 5a.

InstaD can be seen in Figure 6c. It manifests as a small green cross along the diagonal within the GASF image, while it is harder to spot in GADF. Similar to all other GAF transformations, this one also bares a resemblance to RP representation, only that it is less distinct.

The final GAF anomaly representation is SlowD, which is shown in Figure 7c. This is best observed in GADF, where it can be seen that the highest values in the upper left corner of the image. This represents that the values at the beginning of the curve trace are much more similar to each other than the values at the end of the trace. No obvious pattern can be observed in the GASF image.

## V. PROPOSED DNN CLASSIFICATION MODELS

We define our prediction model as function  $\Phi$  depicted in Figure 2 that transforms the input transformed data  $H$  to the set of target classes  $C$  as provided in Equation 8.

$$C = \Phi(H) = \Psi(Z), \text{ where } Z = W \cdot H + B \quad (8)$$

where  $Z$  takes the input data  $H$  and multiplies it with weights and adds bias from the model to it. The activation function  $\Psi$  is then applied to  $Z$  and the predicted class  $C$  is returned.

We have designed two architectures of convolutional neural networks  $\Phi(H)$ , one for binary and the other for the five-class classification. In essence, the same architecture is used for both classification problems, the only difference being the output layer, which is adapted according to the classification type. The two architectures are depicted in Figures 8 and 9 respectively. On the left side of both figures there is an input of

size  $300 \times 300$  pixels, which is the size of the image resulting from transforming the TS. The image is then fed into the neural network, which starts with four convolutional layers. The first layer uses 128 filters with kernel size  $3 \times 3$  pixels. The next three convolutional layers use 64, 32, and 16 filters with a kernel size of  $7 \times 7$ . After the last convolution layer, max-pooling is applied to the output, reducing the height and width of the output by half. The data is then flattened and fed into the dense layer, consisting of 64 nodes, and connected to the output layer, which is either size 2 or 5 depending on the classification type. All hidden layers use the ReLU function that inserts non-linearity into the model and thus helping with the classification of classes with non-linear boundary.

The important part of this model is the activation function of the output layer. Considering a possible real world application scenario, where there could be different combinations of anomalies present within captured time series trace, we used a sigmoid activation function instead of more commonly used softmax function. The reason for that is, because sigmoid function calculates the probability for each class separately, it is more suited for solving problems when outputs are not mutually exclusive.

## VI. METHODOLOGY AND EXPERIMENTAL DETAILS

To present experiment details of our work we first describe dataset generation procedure and then present details of model training and results evaluation.

### A. Dataset generation

For our experimental evaluation, we choose a Rutgers dataset [31] containing real-world measurements and then we synthetically injected anomalies. These traces were then converted into RP, GASF and GADF images. This resulted in 3 datasets for solving our binary and five-class classification problem and comparing the results.

TABLE I  
SYNTHETIC ANOMALY INJECTION METHOD.

Type	Links	Affected	Appearance	Persistence
SuddenD	2 123	33% (700)	once, [200 <sup>th</sup> , 280 <sup>th</sup> ]	for $\infty$
SuddenR			once, [25 <sup>th</sup> , 275 <sup>th</sup> ]	for [5, 20]
InstaD			on $\approx 1\%$ of a link	for 1 datapoint
SlowD			once, [1 <sup>st</sup> , 20 <sup>th</sup> ]	for [150, 180] <sup>†</sup>

<sup>†</sup>  $RSSI(x, \text{start}) \leftarrow RSSI(x) + \min(0, -\text{rand}(0.5, 1.5) \cdot (x - \text{start}))$

The Rutgers dataset consists of link traces from 29 nodes at 5 different noise levels. The dataset contains the raw Received Signal Strength Indicator (RSSI), sequence numbers, source node ID, destination node ID and artificial noise levels. Each RSSI value represents the signal strength of a received packet sent every 100 milliseconds, for a period of 30 seconds. Thus, we obtain traces with a length of 300 RSSI samples.

To inject the anomalies into the Rutgers dataset, we first filtered out samples that did not exhibit packet loss. This left 2123 samples, of which 33% were randomly injected with some kind of anomaly, while the other links were left

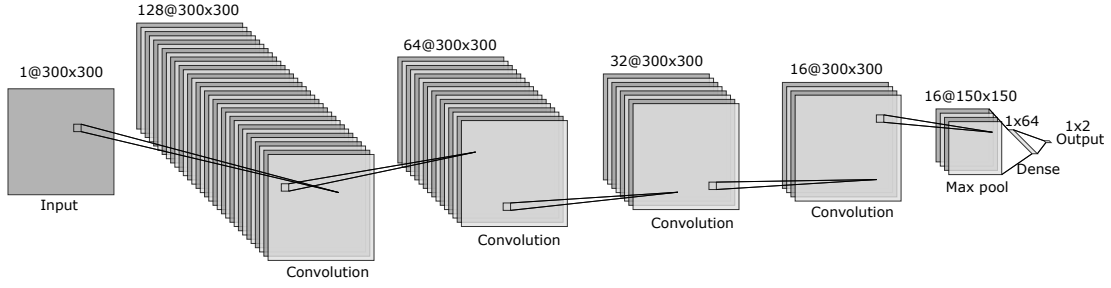


Fig. 8. Deep learning network model for binary detection for GAF and RP

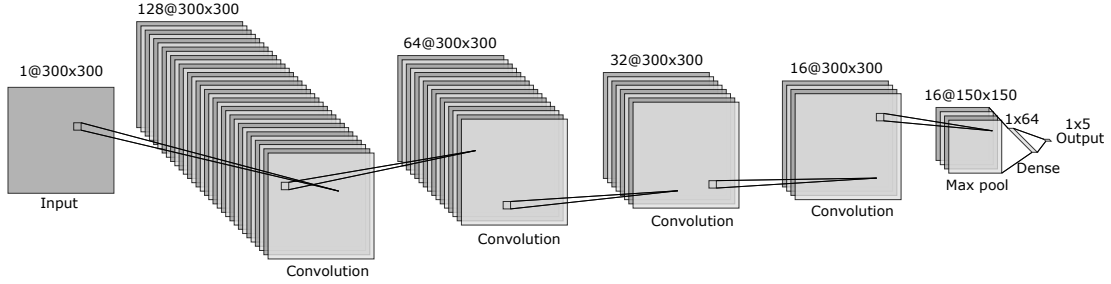


Fig. 9. Deep learning network model for five class anomaly detection for GAF and RP

untouched. The anomalies were randomly injected according to [4] according to the parameters from Table I. This gave us 4 raw time series datasets, one for each of the four anomalies, which together constitute our final dataset. It consists of 8492 samples, with each anomaly represented by 700 samples, while there are a total of 5692 traces that have no anomaly. These traces are then transformed into RP, GASF, and GADF images. In the RP transformation, the Heaviside function and thresholding were omitted as such design decisions gave the best final results.

### B. Model training and evaluation

For training purpose we created a shuffled dataset training and test split with 80:20 ratio, same as in [4] so that the results could be compared. We did the same shuffle split ten times for each model selection. The model is trained on the training set and evaluated on test set so that we can ensure credible results. Because of the imbalanced nature of the dataset, we weighted the classes during training process. The purpose is to penalize the misclassification made by the minority classes by setting a higher class weight and at the same time reducing weight for the majority class. The "No anomaly" class was our majority class and got a weight of 0.1, which is lower than the distribution ratio between anomalous and non anomalous links to ensure greater importance to the anomaly samples, while all other classes were assigned a weight of 1.

We evaluated the models using the standard precision, recall and F1 metrics for each class. The precision measures how many instances detected as class A actually belong to class A, expressed as:  $\text{Precision} = \frac{TP}{TP+FP}$ , while recall measures how many of the instances belonging to class A were actually detected, expressed as:  $\text{Recall} = \frac{TP}{TP+FN}$ , where TP, FP and FN stand for true positives, false positives and false negatives. The F1 score is the harmonic mean between precision and recall,

where larger values indicate better classifiers. We did not use accuracy as a metric because of the unbalanced dataset and as such would bias towards a class with higher representation and be misleading.

We created a baseline model that takes as input the raw time series data with length of 300, and compare its performance to the models developed using the RP and GAF transforms. The first two convolutional layers consist of 64 filters of kernel size 3. The third layer has 32 filters with the same kernel size as previous ones. Final two convolutional layers both use 16 filters of kernel size 7. The output data is then flattened and fed into a dense layer with 64 nodes followed by another dense layer with 32 nodes. Finally, the data is fed into the output layer that can be either of size 2 or 5, depending on the classification type, with sigmoid activation function. All other layers of the network for activation use the ReLU function and do convolution with stride 1. This combination of layers gave the best result while being as simple as possible.

### C. Explainability of the image models

To understand the performance of our best performing RP model, it is important to explain its decisions. One way this can be done is by using Guided Backpropagation [32], which is a way of visualising what image features CNNs detect. This is done by visualizing gradients with respect to the image where only positive values of gradients are used for backpropagating through ReLU layers, while the negative values are set to zero. Doing this, values in the filters of CNNs that are greater than zero signify pixels with higher importance to the recognition and show which pixels in the image contribute the most to the classification. This results in a Guided Backpropagation images, like in Figure 10, where lighter pixels show higher importance to the recognition, while darker pixels show lesser importance.

TABLE II  
CLASSIFICATION RESULTS

Classification	Class	time-value features			recurrence plot			GASF			GADF		
		Prec.	Rec.	F1	Prec.	Rec.	F1	Prec.	Rec.	F1	Prec.	Rec.	F1
Binary	True	0.9	0.86	0.88	0.99	1.00	<b>0.99</b>	0.97	0.98	0.98	0.91	0.92	0.91
	False	0.64	0.72	0.68	0.99	0.96	<b>0.97</b>	0.94	0.93	0.94	0.97	0.97	<b>0.97</b>
Multiclass	SuddenD	1.00	1.00	1.00	0.99	1.00	<b>1.00</b>	0.99	0.99	0.99	1.00	1.00	<b>1.00</b>
	SuddenR	0.98	0.96	0.97	0.99	0.99	<b>0.99</b>	0.99	0.92	0.95	0.98	0.99	0.98
	InstaD	0.97	0.81	0.88	0.93	0.90	<b>0.91</b>	0.92	0.88	0.90	0.90	0.82	0.86
	SlowD	0.62	0.85	0.72	1.00	0.99	<b>0.99</b>	0.95	0.96	0.95 <sup>5</sup>	0.75	0.99	0.85
	No anomaly	0.97	0.95	0.96	0.99	0.99	<b>0.99</b>	0.97	0.99	0.98	0.98	0.96	0.97

## VII. RESULTS

In this section, we evaluate the relative performance of the time series transformations considered in Section IV and the deep learning models proposed in Section V for solving the binary and multi class classification problems formulated in Section III. We also provide the explanation of the model to provide transparency to how the classification is made. The experimental details used to obtain the results are detailed in Section VI.

### A. Performance of image transformation models for binary classification

Table II presents the results of the classifiers. The first two lines of the table list the results of the binary classifier while the last five lines list the results of the multi-class classifier. The first column of the table lists the type of classifier, the second lists the classes while the remaining four columns list the four types of considered input data and the results of the corresponding models using the three selected metrics. According to Table II, the best performing model is based on the RP as also bolded in the corresponding column.

The reason RP model outperforms the GAF models is down to the way transformations are calculated. As explained in the Section VI, while calculating the RP transformation, the thresholding and binarization were omitted which means that none of the information about the time series sample is lost. The images for GASF and GADF transformation are computed from the angles of polar coordinates, while disregarding the information about the amplitude, which means that some of the information about the time series sample is lost, contributing to a worse classification performance compared to RP model.

As it can be seen in the first line of the binary classifier results in Table II the RP model achieves near perfect F1 score of 0.99 in detecting anomalous links. This is slightly better than the 0.98 F1 score of GASF model, while GADF model performs the worst out of the three with the F1 score of 0.91. What can be observed is that all three image models outperform the raw TS model that yields an F1 score of 0.88, which is lower by up to 0.11 compared to the F1 scores of the image based classification models.

What can also be observed from the first row is that the GADF F1 score is lower by 0.07 compared to the GASF model which shows worse performance in detecting anomalies. The

reason for this is due to the ratio between the values in the region of the anomaly and the region around the anomaly which is much higher on average for GASF than for GADF, making the anomalies more prominent for the model to learn. This can best be seen in Figures 4c and 5c respectively.

Compared to the raw TS model, significant improvement in performance is achieved in detecting non anomalous links with image models. Looking at the second line of binary classifier results in Table II it can be seen that both the RP and GADF models perform with an F1 score of 0.97, which is slightly better than the performance of GASF model with F1 score of 0.94. All three models are superior to raw TS model which achieved an F1 score of 0.68.

### B. Performance of image transformation models for multiclass classification

In the lower part of the Table II the last five lines list the results of the multi-class classifier, where the best performing model is based on the RP as also bolded in the corresponding column. To provide additional insights into the classification decisions, in Figure 10 we provide explanation maps of a randomly extracted sample for each anomaly from the testing dataset.

The general observations regarding the performance of the image based models are similar to the ones seen in Section VII-A. In general GASF model is better at detecting anomalies than GADF model, while RP is the best image based model, the reasons for both observations being the same as explained in the Section VII-A. Finally, according to the F1 scores all image models outperform the TS model, where the F1 scores can be higher by up to 0.27.

As it can be seen in the first line of the multi-class classifier results in Table II, all three imaging models perform very well in predicting the SuddenD anomaly, with the RP and GADF models having an F1 score of 1.00, while the F1 score of GASF is 0.99. All three results are similar to or even slightly better than the baseline raw TS model. As it can be observed in Figure 10a for detecting the SuddenD anomaly the model focuses on the black parts of the image seen in the example Figure 4b. This also complies with synthetic injection approach from Table I, where SuddenD anomaly is observed towards the end of the window of the time series.

Looking at the second row of the multi-class classifier results in Table II, there is a slight drop in performance in



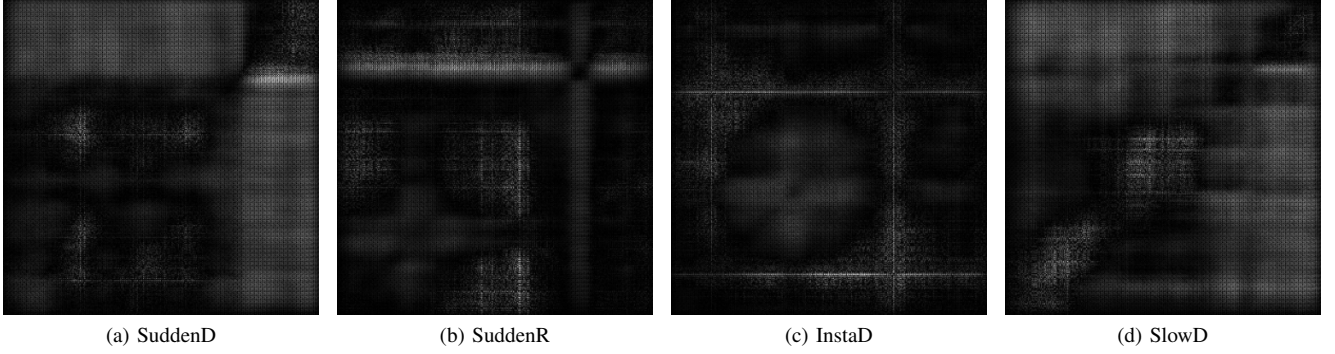


Fig. 10. Distinct representations of explanations of model decisions acquired by Guided Backpropagation.

SuddenR detection compared to SuddenD. The best performing model is the RP model with F1 score of 0.99, followed by GADF with an F1 score of 0.98. Considering the F1 score of 0.97 of the raw TS model, both the RP and GADF models perform with a higher F1 score than the baseline model, while GASF with F1 score of 0.95 slightly under-performs compared to the raw TS model.

In the third row of the of the multi-class classifier results in Table II, the performance of the InstaD classifier can be observed. Again, with an F1 score of 0.91, RP model performs the best out of all image models, while the GASF model with an F1 score of 0.90 is a close second. Together, they outperform the 0.88 F1 score of the raw TS baseline model, while the GADF model with F1 score of 0.86 slightly underperforms compared to the baseline model. Figures 10b and 10c representing the explanation maps for the SuddenD and InstaD anomalies show that for the respective anomalies the model focuses on black cross-like areas similar to the typical representations in Figures 5b and 6b. Since SuddenR and InstaD can randomly occur anywhere along the time series length, as shown in Table I, some activation can also be seen in other parts of the figures, to help determine the anomaly.

According to the fourth line of the of the multi-class classifier results in Table II, compared to the 0.95 F1 score of the GASF model and 0.85 F1 score of the GADF model, the RP model is the best performing model with an F1 score of 0.99. All three models significantly outperform the 0.72 F1 score of the raw TS baseline model. The explanation map of the final anomaly, SlowD, is presented in the Figure 10d. As it can be seen the most important parts of the images are along the upper and right edge. This shows that the model is most focused on the last part of the anomaly trace where the values are lower compared to the beginning of the trace, as seen in Figure 7a, and also results in higher density area in Figure 7b along the top and right edge of the figure.

In the last row of the of the multi-class classifier results in Table II, performance results of classifying links without anomaly are presented. Like in all of the previous rows also here the RP model with an F1 score of 0.99 is again, compared to the 0.98 F1 score of the GASF model and 0.97 F1 score of the GADF model, the best performing image model. All three models outperform the baseline model which achieved and F1 score of 0.96.

### C. Comparison to the state of the art

Since the performance of the recurrence plot model was superior to other two proposed models, we chose to compare it to the ensemble learner consisting of the best single class classifiers designed by [4]. We used the same testing data that we used for testing our models. The comparison can be seen in Table III. The first column lists the classes while the remaining two columns lists ensemble model from [4] and our best performing RP model using the three selected metrics.

TABLE III  
COMPARISON OF RESULTS BETWEEN OUR MODEL AND THE STATE OF THE ART IN [4]

Class	Ensamble learner from [4]			Our best result		
	Prec.	Rec.	F1	Prec.	Rec.	F1
SuddenD	1.00	1.00	<b>1.00</b> <sup>5</sup>	0.99	1.00	<b>1.00</b> <sup>6</sup>
SuddenR	0.49	0.67	0.56 <sup>1</sup>	0.99	0.99	<b>0.99</b> <sup>2</sup>
InstaD	0.31	0.42	0.36 <sup>1</sup>	0.93	0.90	<b>0.91</b> <sup>1</sup>
SlowD	0.54	0.81	0.65 <sup>5</sup>	1.00	0.99	<b>0.99</b> <sup>2</sup>
No anomaly	0.93	0.87	0.90	0.99	0.99	<b>0.99</b>

From the table it can be seen that with the exception of the SuddenD anomaly detection, our model outperforms their ensemble learner in all other classes. The paper showed the potential of such models but this result shows that those trained models are not yet ready for use in production because they have trouble performing when put into an ensemble. They made assumptions that only isolated cases of various anomalies can appear on links, which is not entirely aligned with a realistic environment where various anomalies can appear simultaneously. Due to these assumptions, the classifiers put into an ensemble can classify anomalies, that are not their own, as false positive. This goes to show that our model is more robust when it comes to an unseen mix of anomalies, compared to the model from [4].

## VIII. CONCLUSION

In this paper, we performed a first time analysis of image-based representation techniques for wireless anomaly detection using recurrence plots and Gramian angular fields for binary and multi-class classification and proposed a new deep neural network architecture that is able to distinguish between the

considered wireless link layer anomalies. Our results show that the best performing model developed using the recurrence plot transformation outperforms the other image-based models by up to 14%, and improves performance of anomaly detection by up to 29% for binary classification and by up to 27% for multiclass classification compared to a raw time-series based model. We also show how decisions taken by the model can be explained, which further proves that our model focuses on the main characteristics of each anomaly. We also compared our best performing RP model to the state of the art classical machine learning based ensemble model and showed that although their models show potential, our model is more robust in detecting unseen anomalies outperforming their ensemble by up to 55%.

## REFERENCES

- [1] J. Davies and C. Fortuna, *The Internet of Things: From Data to Insight*. John Wiley & Sons, 2020.
- [2] T. Gale, T. Šolc, R.-A. Moşoi, M. Mohorčič, and C. Fortuna, "Automatic detection of wireless transmissions," *IEEE Access*, vol. 8, pp. 24 370–24 384, 2020.
- [3] G. Cerar, H. Yetgin, M. Mohorčič, and C. Fortuna, "Machine learning for wireless link quality estimation: A survey," *IEEE Communications Surveys Tutorials*, pp. 1–1, 2021.
- [4] G. Cerar, H. Yetgin, and C. Fortuna, "Learning to Detect Anomalous Wireless Links in IoT Networks," in *IEEE Access*, 2020, pp. 363–368.
- [5] J. D. C. Silva, J. J. P. Rodrigues, K. Saleem, S. A. Kozlov, and R. A. Rabêlo, "M4DN. IoT-A Networks and Devices Management Platform for Internet of Things," *IEEE Access*, vol. 7, pp. 53 305–53 313, April 2019.
- [6] A. Sheth, C. Doerr, D. Grunwald, R. Han, and D. Sicker, "Mojo: A distributed physical layer anomaly detection system for 802.11 wlns," in *Proceedings of the 4th international conference on Mobile systems, applications and services*. ACM, 2006, pp. 191–204.
- [7] V. L. Thing, "IEEE 802.11 network anomaly detection and attack classification: A deep learning approach," in *IEEE Wireless Communications and Networking Conference (WCNC)*, San Francisco, CA, USA, March 2017.
- [8] J. Ran, Y. Ji, and B. Tang, "A semi-supervised learning approach to ieee 802.11 network anomaly detection," in *2019 IEEE 89th Vehicular Technology Conference (VTC2019-Spring)*. IEEE, 2019, pp. 1–5.
- [9] Z. Chen, C. K. Yeo, B. S. Lee, and C. T. Lau, "Autoencoder-based network anomaly detection," in *2018 Wireless Telecommunications Symposium (WTS)*, 2018, pp. 1–5.
- [10] T. Luo and S. G. Nagarajan, "Distributed anomaly detection using autoencoder neural networks in wsn for iot," in *2018 IEEE International Conference on Communications (ICC)*, 2018, pp. 1–6.
- [11] S. Gupta, R. Zheng, and A. M. Cheng, "Andes: an anomaly detection system for wireless sensor networks," in *2007 IEEE International Conference on Mobile Adhoc and Sensor Systems*, 2007, pp. 1–9.
- [12] A. Krizhevsky, I. Sutskever, and G. E. Hinton, "Imagenet classification with deep convolutional neural networks," *Advances in neural information processing systems*, vol. 25, pp. 1097–1105, 2012.
- [13] Z. Zhao, P. Zheng, S. Xu, and X. Wu, "Object detection with deep learning: A review," *IEEE Transactions on Neural Networks and Learning Systems*, vol. 30, no. 11, pp. 3212–3232, 2019.
- [14] M. S. Singh, V. Pondenkandath, B. Zhou, P. Lukowicz, and M. Liwicki, "Transforming sensor data to the image domain for deep learning — an application to footprint detection," in *2017 International Joint Conference on Neural Networks (IJCNN)*, 2017, pp. 2665–2672.
- [15] A. Sharma, E. Vans, D. Shigemizu, K. A. Boroevich, and T. Tsunoda, "DeepInsight: A methodology to transform a non-image data to an image for convolution neural network architecture," *Scientific Reports*, vol. 9, no. 1, Aug. 2019. [Online]. Available: <https://doi.org/10.1038/s41598-019-47765-6>
- [16] Z. Wang and T. Oates, "Encoding time series as images for visual inspection and classification using tiled convolutional neural networks," in *Workshops at the twenty-ninth AAAI conference on artificial intelligence*, vol. 1, 2015.
- [17] J. Eckmann, S. O. Kamphorst, D. Ruelle *et al.*, "Recurrence plots of dynamical systems," *World Scientific Series on Nonlinear Science Series A*, vol. 16, pp. 441–446, 1995.
- [18] M. Långkvist, L. Karlsson, and A. Loutfi, "A review of unsupervised feature learning and deep learning for time-series modeling," *Pattern Recognition Letters*, vol. 42, pp. 11–24, 2014.
- [19] A. Bagnall, J. Lines, A. Bostrom, J. Large, and E. Keogh, "The great time series classification bake off: a review and experimental evaluation of recent algorithmic advances," *Data Mining and Knowledge Discovery*, vol. 31, no. 3, pp. 606–660, May 2017. [Online]. Available: <http://link.springer.com/10.1007/s10618-016-0483-9>
- [20] Z. Xing, J. Pei, and E. Keogh, "A brief survey on sequence classification," *ACM Sigkdd Explorations Newsletter*, vol. 12, no. 1, pp. 40–48, 2010.
- [21] H. Ismail Fawaz, G. Forestier, J. Weber, L. Idoumghar, and P.-A. Muller, "Deep learning for time series classification: a review," *Data Mining and Knowledge Discovery*, vol. 33, no. 4, pp. 917–963, Jul. 2019. [Online]. Available: <http://link.springer.com/10.1007/s10618-019-00619-1>
- [22] H. Bousbiat, C. Klemenjak, and W. Elmenreich, "Exploring time series imaging for load disaggregation," in *Proceedings of the 7th ACM International Conference on Systems for Energy-Efficient Buildings, Cities, and Transportation*, 2020, pp. 254–257.
- [23] Y. Choi, H. Lim, H. Choi, and I. Kim, "Gan-based anomaly detection and localization of multivariate time series data for power plant," in *2020 IEEE International Conference on Big Data and Smart Computing (BigComp)*, 2020, pp. 71–74.
- [24] G. Krummenacher, C. S. Ong, S. Koller, S. Kobayashi, and J. M. Buhmann, "Wheel defect detection with machine learning," *IEEE Transactions on Intelligent Transportation Systems*, vol. 19, no. 4, pp. 1176–1187, 2018.
- [25] G. Zhang, Y. Si, D. Wang, W. Yang, and Y. Sun, "Automated Detection of Myocardial Infarction Using a Gramian Angular Field and Principal Component Analysis Network," *IEEE Access*, vol. 7, pp. 171 570–171 583, 2019. [Online]. Available: <https://ieeexplore.ieee.org/document/8911378/>
- [26] H. Xu, J. Li, H. Yuan, Q. Liu, S. Fan, T. Li, and X. Sun, "Human Activity Recognition Based on Gramian Angular Field and Deep Convolutional Neural Network," *IEEE Access*, vol. 8, pp. 199 393–199 405, 2020. [Online]. Available: <https://ieeexplore.ieee.org/document/9234451/>
- [27] D. F. Silva, V. M. A. D. Souza, and G. E. A. P. A. Batista, "Time series classification using compression distance of recurrence plots," in *2013 IEEE 13th International Conference on Data Mining*, 2013, pp. 687–696.
- [28] M. Hu, X. Feng, S. Zhou, and W. Xu, "Anomaly Detection in Time Series Data Based on Unthresholded Recurrence Plots," in *International Conference on Applications and Techniques in Cyber Security and Intelligence ATCI 2018*, J. Abawajy, K.-K. R. Choo, R. Islam, Z. Xu, and M. Atiquzzaman, Eds. Cham: Springer International Publishing, 2019, pp. 477–484.
- [29] Y. Chen, S. Su, and H. Yang, "Convolutional neural network analysis of recurrence plots for anomaly detection," *International Journal of Bifurcation and Chaos*, vol. 30, no. 01, p. 2050002, 2020. [Online]. Available: <https://doi.org/10.1142/S0218127420500029>
- [30] L. Kirichenko, P. Zinchenko, T. Radivilova, and M. Tavalbeh, "Machine learning detection of ddos attacks based on visualization of recurrence plots," *nonlinear dynamics*, vol. 1000, p. 1, 2019.
- [31] S. K. Kaul, I. Seskar, and M. Gruteser, "CRAWDAD dataset Rutgers/noise (v. 2007-04-20)," Downloaded from <https://crawdad.org/rutgers/noise/20070420/RSSI>, Apr. 2007, traceset: RSSI.
- [32] J. Springenberg, A. Dosovitskiy, T. Brox, and M. Riedmiller, "Striving for simplicity: The all convolutional net," in *ICLR (workshop track)*, 2015.